How to Prepare Kinetically Stable Self-assembled $Pt_{12}L_{24}$ Nanocages while Circumventing Kinetic Traps

Eduard O. Bobylev,[a] David A. Poole, III,[a] Bas de Bruin,[a] and Joost N. H. Reek*[a]

Abstract: Supramolecular coordination-based self-assembled nanostructures have been widely studied, and currently various applications are being explored. For several applications, the stability of the nanostructure is of key importance, and this strongly depends on the metal used in the self-assembly process. Herein, design strategies and synthetic protocols to access desirable kinetically stable $Pt_{12}L_{24}$ nanospheres are reported, and it is demonstrated that these are stable under conditions under which the palladium counterparts decompose. Descriptors previously used for palladium nanospheres are insufficient for platinum analogues, as the stronger metal–ligand bond results in a mixture of kinetically trapped structures. We report that next to the dihedral angle, the rigidity of the ditopic ligand is also a key parameter for the controlled formation of $Pt_{12}L_{24}$ nanospheres. Catalytic amounts of coordinating additives to labilise the platinum-pyridyl bond to some extent are needed to selectively form $Pt_{12}L_{24}$ assemblies. The formed $Pt_{12}L_{24}$ nanospheres were demonstrated to be stable in the presence of chloride, amines and acids, unlike the palladium analogues.

Introduction

Supramolecular coordination-based self-assembled nanostructures have a potentially rich diversity of applications including drug delivery,[1] containers for catalytic transformations,[2] separation vehicles[3] and many more.[4] In general, the properties of supramolecular structures are unique in comparison to the components they are based on, most often because of the three dimensional structure that is generated, creating specific spaces and organising molecular components.[5] Therefore, it is important that the coordination-based supramolecular nanostructures are stable under the conditions required for applications such as catalysis, guest binding and separation and *in vivo* applications.[2c–e,4b,6] Strategies to enhance the stability of coordination-based self-assemblies are generally based on increasing the metal-ligand bond strength, which can be achieved by changes in the ligand system or by using a different metal site. Examples that led to more robust assemblies by ligand design include changes in the electronical properties of the donation site and changes in the steric properties.[1c,7] Changing the metal site might lead to more robust assemblies when known building blocks are used, without changing too much the overall structure. Prominent examples include the change of iron to nickel in tetrahedral M_4L_6 assemblies,[8] the change from copper to rhodium in M_4L_4-type assemblies[9] and the change of palladium to platinum in M_2L_4 assemblies (Figure 1).[10]

The power of the formation of coordination-based supramolecular self-assemblies is that it is based on reversible bonds and as such it proceeds through repair of wrongly formed bonds to produce the thermodynamically controlled desired product. This is particularly important if the assembly is based on a large number of components, which is the case for $M_{12}L_{24}$ nanospheres. The quest for more stable structures by

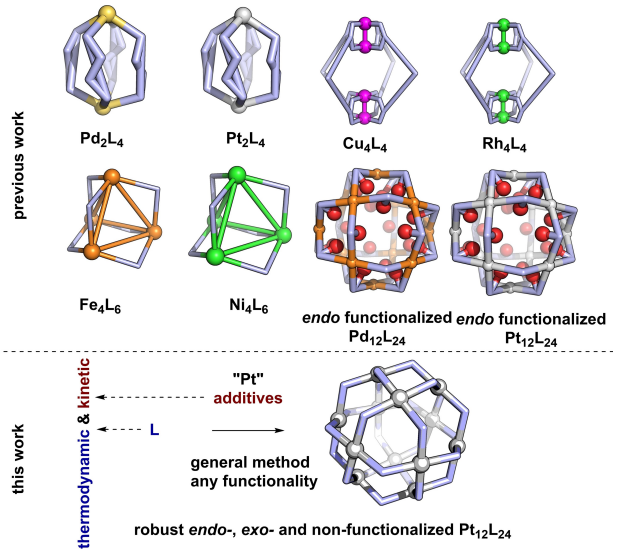

Figure 1. Schematic representation of different types of assemblies whose stability was greatly enhanced by changing the metal (ligands displayed in light blue, metal centres as spheres).

[a] E. O. Bobylev, D. A. Poole, III, Prof. Dr. B. de Bruin, Prof. Dr. J. N. H. Reek
Supramolecular and Homogeneous Catalysis Group, van't Hoff Institute for Molecular Sciences
University of Amsterdam
Science Park 904, 1098 XH Amsterdam (the Netherlands)
E-mail: j.n.h.reek@uva.nl

Supporting information for this article is available on the WWW under https://doi.org/10.1002/chem.202101931

using stronger bonds between the metal and ligand therefore comes with the challenge of selective formation of the thermodynamically most stable assembly, while preventing the formation of kinetically trapped species and undesired intermediates.[6] Motivated by this challenge, we studied how robust $Pt_{12}L_{24}$ nanospheres can be generated based on $Pd_{12}L_{24}$ assemblies, taking both thermodynamic and kinetic arguments into account. We introduce the ligand flexibility parameter that can be used in the design, by which kinetic traps can be overcome.

Palladium-based M_nL_{2n} assemblies are formed by complexation of a building block containing two pyridine moieties that are oriented with a certain dihedral angle. Four pyridine moieties coordinate to the metal site in a square planar geometry.[11] This quantitively yields Pd_nL_{2n} spheres as the thermodynamic most favourable structure. This type of Pd_nL_{2n} assemblies were shown to provide highly versatile materials as they can be easily functionalised on both the outside (*exo*) or the inside (*endo*). *Endo* functionalisation can lead to preorganisation of up to 24 functional groups inside of $Pd_{12}L_{24}$ spheres, yielding ideal systems to study cooperativity effects.[2c–e,12] Through the implementation of different functional groups on the outside of Pd_nL_{2n} assemblies, functional materials and even gels can be prepared.[13] Some of these structures were shown to be able to interact with biological components (such as proteins, enzymes and DNA),[14] providing an opening for applications in biology. Given the huge variety of applications of Pd_nL_{2n} spheres, the extension to more stable analogues is desirable as it might lead to an even broader scope of applications. The most obvious strategy is the preparation of platinum-based analogues, and indeed some examples have been reported.[2d,e,4b,6,10a,12,15] Next to Pt_6L_{12}, which was reported and crystalised earlier by Fujita et al.,[6] we recently have shown that $Pt_{12}L_{24}$ assemblies are formed through a set of kinetically stable intermediates with the general formula Pt_nL_{2n} for $n=6$–11 (Figure 2).[15a] Using only the design principles developed for palladium-based assemblies, that is taking the dihedral angle between the pyridine donors as a guide for the prediction of the formation of the nanosphere, was insufficient for platinum nanospheres. Building blocks that were predicted to provide $Pt_{12}L_{24}$ nanospheres yielded a mixture of different assemblies such as Pt_8L_{16}, Pt_9L_{18} and the desired $Pt_{12}L_{24}$ assembly, even when reacted at high temperature (150 °C). The kinetically trapped states were too stable and could not be converted to the desired $Pt_{12}L_{24}$ nanosphere. These trapped states were destabilised by introducing a bulky group or a positively charged moiety at the *endo* site of the building block (Figure 1), which resulted in selective formation of the $Pt_{12}L_{24}$ nanospheres. Based on the successful destabilisation strategy of intermediates, we were motivated to develop a general ligand approach using design principles, rather than functionalisation, to achieve selective formation of self-assemblies with strong metal-ligand bonds.

Results and Discussion

During the formation of platinum-based $Pt_{12}L_{24}$ assemblies, some Pt_nL_{2n} assemblies for $n=6$–11 have been recently identified as trapped intermediates.[15a] A comparison of the modelled structures $Pt_8\mathbf{L}^{\mathbf{OMe}}{}_{16}$, $Pt_9\mathbf{L}^{\mathbf{OMe}}{}_{18}$ and the desired $Pt_{12}\mathbf{L}^{\mathbf{OMe}}{}_{24}$ assembly shows a difference in dihedral angle of the ditopic ligand building block for various structures that deviates from the natural ligand dihedral angle (Figure 2). Whereas the dihedral angle between the pyridine donors is close to the preferred 120° arrangement in the free building block and in the $Pt_{12}L_{24}$ assemblies, it is distorted to 110° or 115° for the analogue Pt_8L_{16} and Pt_9L_{18}. Destabilisation of these intermediate structures can therefore be achieved by increasing the deformation energy required to bend the building block from

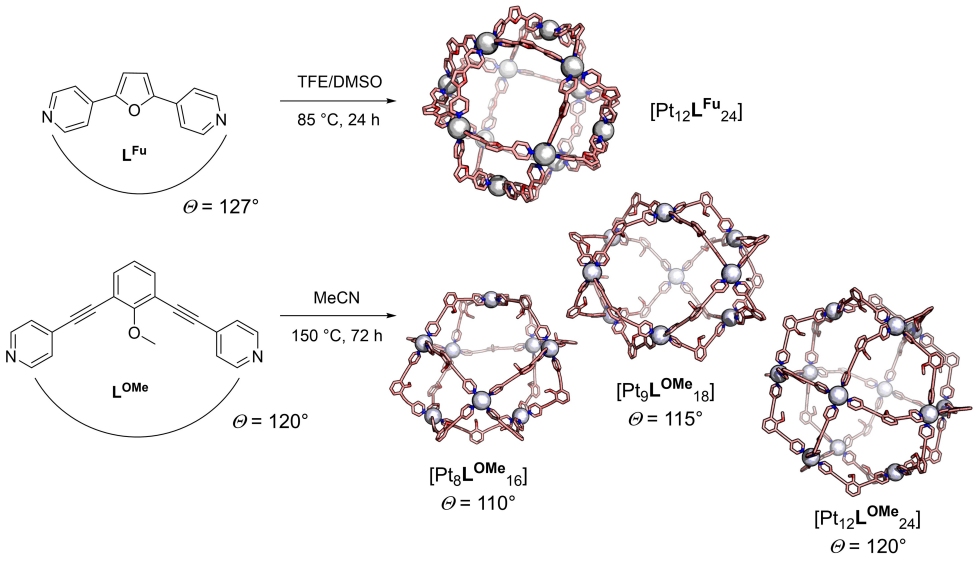

Figure 2. Example of trapped $Pt_8\mathbf{L}^{\mathbf{OMe}}{}_{16}$ and $Pt_9\mathbf{L}^{\mathbf{OMe}}{}_{18}$ and the averaged dihedral angle requirements.

the preferred 120°, in a similar manner as reported previously for $Pd_{15}L_{30}$ assemblies.[11b] For this reason, we propose not only to calculate the dihedral angle, but also the flexibility range of a building block, which we define as accessible dihedral angle window within 2 kcal/mol energy penalty. It is anticipated that rigid building blocks, with a small flexibility range, will destabilise the intermediates to a larger extend. To investigate this, the dihedral angle and flexibility range for three electronically similar building blocks were evaluated using DFT (Section SI6): the acetylene-linked $\mathbf{L}^{\mathbf{OMe}}$ building block, a building block that has no linker in between the central benzene ring and the pyridine donors ($\mathbf{L}^{\mathbf{SOMe}}$) and a building block with a 1,4-phenylene linker in between ($\mathbf{L}^{\mathbf{BnPy}}$). The flexibility range of $\mathbf{L}^{\mathbf{OMe}}$ is within 2 kcal/mol from 95°–146° (Figure 3). In comparison to that, the two other building blocks $\mathbf{L}^{\mathbf{BnPy}}$ and $\mathbf{L}^{\mathbf{SOMe}}$ allow only access to dihedral angles ranging from 106° to 133° (145°; Figure 3). We therefore identified $\mathbf{L}^{\mathbf{SOMe}}$ as the most rigid building block and $\mathbf{L}^{\mathbf{BnPy}}$ as moderately rigid and $\mathbf{L}^{\mathbf{OMe}}$ as flexible.

To evaluate how the flexibility range influences the relative stability of the $Pt_{12}L_{24}$ compared to previously found intermediates Pt_nL_{2n} for $n=6$–11, modelling was performed using molecular mechanics (Section SI6). The thermodynamically most favoured structure was found to be the $Pt_{12}L_{24}$ assembly in all cases. Because the thermodynamic energy of different sized assemblies is relatively similar for the flexible building block

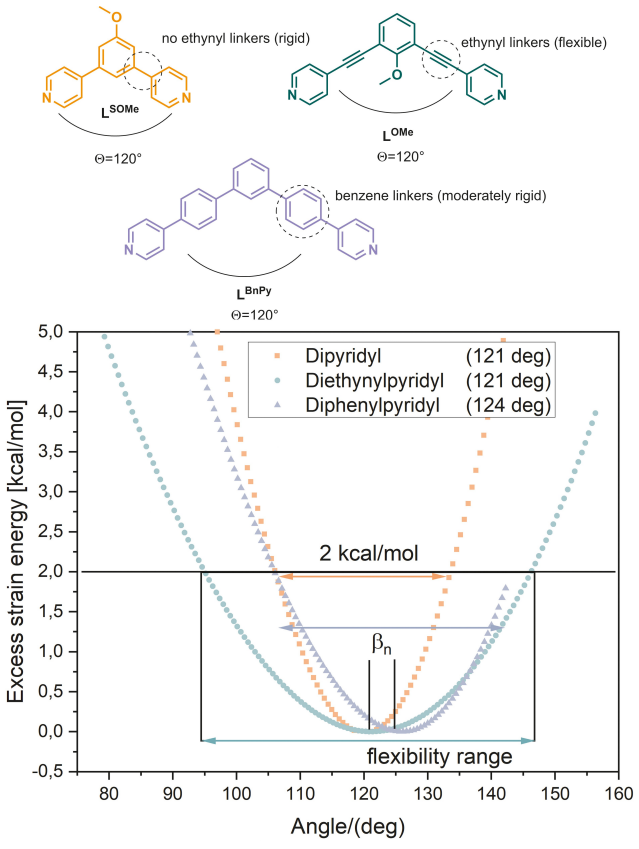

Figure 3. Structure of the building blocks investigated. Energy surface for vertical bending of the pyridine donors computed by relaxed scan of the dihedral angle at the B3LYP/def2TZV level of theory.

$\mathbf{L}^{\mathbf{OMe}}$ selective formation of the desired assembly might be not possible under thermodynamic control (as supported by previous experiments).[15a] The 1,4-phenylene linked building block $\mathbf{L}^{\mathbf{BnPy}}$ shows a similar energy profile as the ethynyl linked building block $\mathbf{L}^{\mathbf{OMe}}$, with even a smaller difference between differently sized assemblies (Figure 4). This building block was found thus to be not suitable for selective sphere formation as similar results as obtained for $\mathbf{L}^{\mathbf{OMe}}$ are expected. For the most rigid building block $\mathbf{L}^{\mathbf{SOMe}}$, the relative energy of small sized spheres for $n=6$–11 is significantly higher than for the $Pt_n\mathbf{L}^{\mathbf{OMe}}{}_{2n}$ analogues (Figure 4). In the case of $\mathbf{L}^{\mathbf{OMe}}$ and $\mathbf{L}^{\mathbf{BnPy}}$, the Pt_9L_{18} spheres are energetically close to the $Pt_{12}L_{24}$ assembly with a difference of 1.5–1.6 kcal/mol. In contrast to that, for $\mathbf{L}^{\mathbf{SOMe}}$, the $Pt_{11}L_{22}$ assembly is energetically the second most favoured structure, with a difference of 6 kcal/mol with respect to the $Pt_{12}L_{24}$ assembly. Having demonstrated on the basis of theoretical models that small sized assemblies are thermodynamically destabilised for the rigid $\mathbf{L}^{\mathbf{SOMe}}$ building block due to a higher deformation penalty, we decided to build on these promising results in the context of selective $Pt_{12}L_{24}$ sphere formation in subsequent experimental investigations.

Two building blocks $\mathbf{L}^{\mathbf{SOMe}}$ and $\mathbf{L}^{\mathbf{BnPy}}$ were investigated experimentally, and compared to sphere formation experiments with $\mathbf{L}^{\mathbf{OMe}}$. Sphere formation experiments were performed by mixing 1 equiv. of building block with 0.6 equiv $[Pt(BF_4)_2(MeCN)_4]$ in acetonitrile, stirring the solution at 150 °C for a certain amount of time. Sphere formation experiments under these conditions using $\mathbf{L}^{\mathbf{BnPy}}$ led to formation of ill-defined material with broad ^{1}H NMR signals (Figure S34 in the Supporting Information). Mass spectroscopy (MS) analysis showed no presence of spherical structures, in line with formation of dominantly oligomeric or polymeric material. In a similar experiment using $\mathbf{L}^{\mathbf{SOMe}}$, a downfield shift of the pyridine protons of $\mathbf{L}^{\mathbf{SOMe}}$ and a general broadening of the ^{1}H NMR signals were observed, in line with cage formation (Figure 5, below). To obtain insights into the structures formed for $\mathbf{L}^{\mathbf{SOMe}}$, the reaction mixture was analysed by high-resolution electrospray ionisation mass spectrometry (HRMS-ESI). The sample shows characteristic signals attributed to $[Pt_n\mathbf{L}^{\mathbf{SOMe}}{}_{2n}]^{x+}$ for $n=$ 8–12 with matching isotopic pattern, indicating that a mixture of sphere structures has been formed under these conditions (Figures S14 and S15, calibration Section SI7). The relative intensity of unique signals attributed to the five assemblies is similar to what has been observed for $\mathbf{L}^{\mathbf{OMe}}$ (Figure 5, below). Characteristic differences in comparison to the more flexible $\mathbf{L}^{\mathbf{OMe}}$ ligand are that the rigid building block $\mathbf{L}^{\mathbf{SOMe}}$ yields more of the larger spheres (such as $Pt_{10}\mathbf{L}^{\mathbf{SOMe}}{}_{20}$ and $Pt_{11}\mathbf{L}^{\mathbf{SOMe}}{}_{22}$) and none of the small assemblies (such as $Pt_6\mathbf{L}^{\mathbf{SOMe}}{}_{12}$; Figure 5, below). This observation is in line with the hypothesis that more rigid linkers have higher deformation energies to form the smaller spheres, thereby destabilising these assemblies. As the calculations predict a large thermodynamic difference between the $Pt_{12}\mathbf{L}^{\mathbf{SOMe}}{}_{24}$ nanosphere and the smaller sized assemblies, these smaller structures most likely represent kinetically trapped species (Figure 4). A selective formation of the $Pt_{12}\mathbf{L}^{\mathbf{SOMe}}{}_{24}$ nanosphere can therefore be possible by using conditions in which the conversion of smaller structures to the $Pt_{12}\mathbf{L}^{\mathbf{SOMe}}{}_{24}$

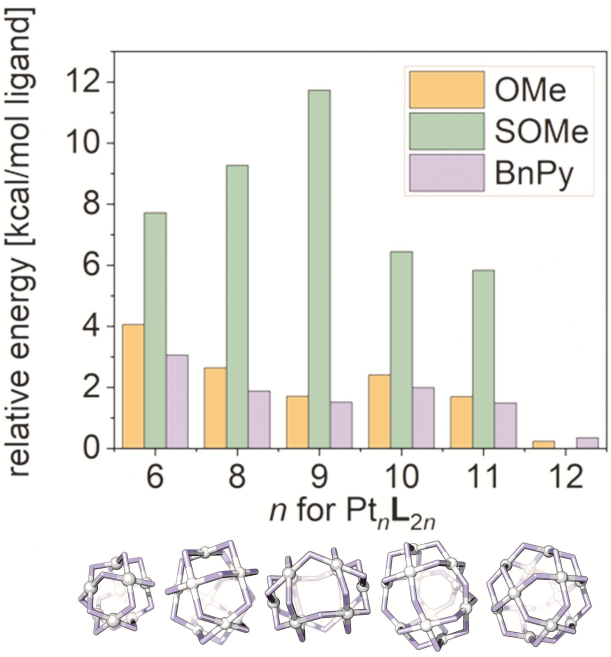

Figure 4. Schematic representation of different types of Pt_nL_{2n} assembly and relative energies of different sized Pt_nL_{2n} assemblies for L^{OMe} [x] L^{SOMe} and L^{BnPy}.

nanosphere is kinetically possible. This was explored by changing the reaction conditions such as temperature, reaction time, solvent and the use of additives. When sphere formation was carried out at higher temperature (e.g., at 170 °C; Figures S12 and S14), the signals in ^{1}H NMR spectrum of the reaction mixture were broader and analysis of the mixture by in HRMS-ESI indicated that the $Pt_{12}\mathbf{L}^{\mathbf{SOMe}}{}_{24}$ sphere was present in lower concentration, suggesting decomposition of the structures before the thermodynamic equilibrium has reached. Longer reaction times at 150 °C did not change the distribution (up to 10 days). Also sphere formation experiments carried out in other solvent showed to be unproductive due to the instability of the solvents at high temperature (DMSO, DMF) or just because the solvent did not change the ligand exchange dynamics ($MeNO_2$, $CDCl_3$). As shown previously, platinum-nitrogen bonds can be destabilised by using UV radiation.[16] Unfortunately, due to a conjugation of the pyridine donors to an aromatic ring, alterative decay pathways without breaking the platinum-pyridine bond are possible. Because we did not want to change the ligand design, an alternative strategy was envisioned based observations made for palladium-based $Pd_{12}L_{24}$ nanospheres. These types of structures appear to show poor stability in the presence of biologically relevant components found in the cytoplasm of living cells, such as amines, thiols, acids and halides.[7,17] These biological substrates are able to coordinate to the palladium centre and when present in higher quantities they can destroy the self-assemblies. Whereas this property is typically not desired for palladium assemblies, when used as additive they may just labilise the platinum–nitrogen bond to the extent that the kinetic intermediates can be converted to the thermodynamic product. We therefore anticipated that the same components relevant to living cells that destroy palladium-based self-assemblies might enhance the dynamicity of platinum-assemblies when added in catalytic amounts, thus potentially driving the selectivity towards the desired thermodynamically favoured structures.

We included in our studies the effect of water on the self-assembly process as well as typically found biological functional groups (amine, carboxylic acid, imidazole, chloride, thiol) in catalytic amounts (Figure 5). As a reference we also included the previously reported TFE/DMSO system that was also reported to be a good combination for the preparation of Pt-

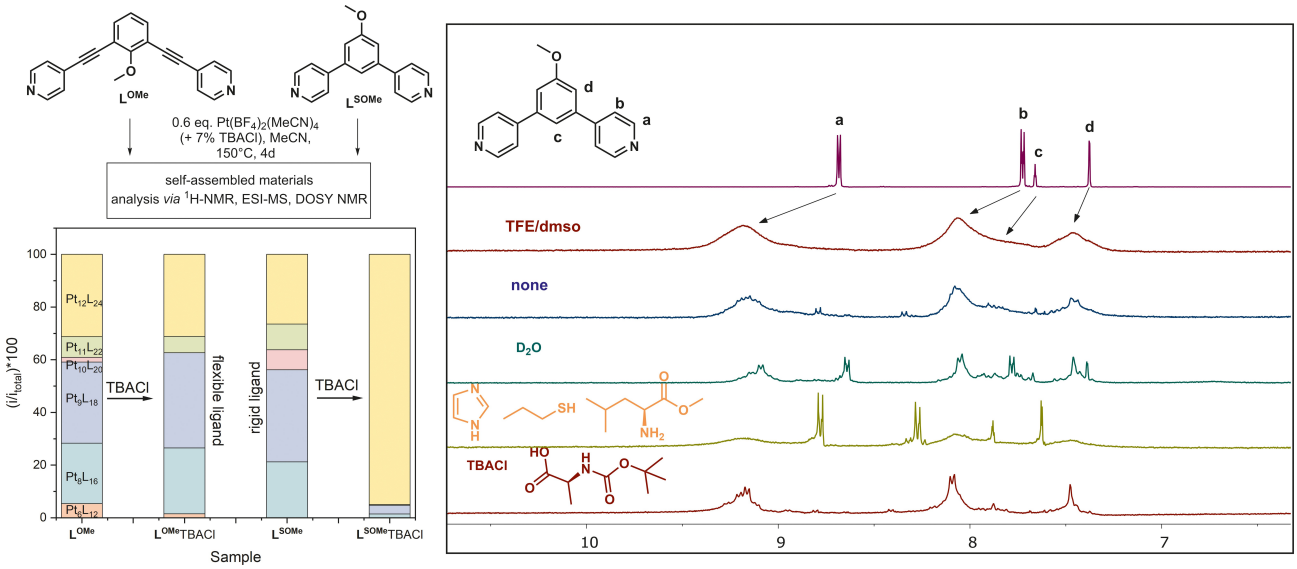

Figure 5. Top left: General conditions of sphere formation using L^{OMe} and L^{SOMe}. Bottom left: Distribution of different sized assemblies for the ligands determined by ESI-MS analysis. Right: Representative ^{1}H NMR spectra (in MeCN) of L^{SOMe} sphere formation using different types of additives (7 mol% with respect to Pt). All sphere formation was performed at 150 °C except for the literature TFE/DMSO system, which was performed at 85 °C.

based assemblies.[6] The additive must labilise the metal-ligand bond (to a larger extend than the solvent), but should not coordinate too strongly as then it becomes competitive for pyridyl coordination, leading to ill-defined materials. First, the effect of the water content was studied. After heating the ligand $\mathbf{L}^{\mathbf{SOMe}}$ and platinum precursor at 150 °C for 4 days in [D_3]MeCN/D_2O (9:1), free ligand was still in the solution (as indicated by the ^{1}H NMR; Figure 5). Apparently, the presence of water hampers sphere formation, and as such all other reactions were performed in high pressure tubes under N_2 with dry degassed solvent. The sample prepared in TFE/DMSO at 85 °C was precipitated in Et_2O and redissolved in CD_3CN for further analysis. The TFE/DMSO sample showed a similar broad ^{1}H NMR spectrum as the sample prepared in pure MeCN (Figure 5) indicating the presence of oligomeric material in solution. Furthermore, HRMS-ESI analysis of the TFE/DMSO sample showed no typical signals associated with nanospheres or kinetically trapped intermediates (Section SI7 and Figure S19). Reactions performed in MeCN at 150 °C in the presence of catalytic amounts of imidazole, amine or thiol displayed ill-defined ^{1}H NMR spectra with some free ligand still present (e.g., Figures 5 and S23). Only small amounts of $Pt_{12}\mathbf{L}^{\mathbf{SOMe}}{}_{24}$ nanospheres and kinetically trapped intermediates were formed according to the HRMS-ESI spectra taken from the samples, in a similar ratio as in the absence of these additives. The rather broad ^{1}H NMR signals together with the low intensity of spherical compounds in HRMS-ESI suggest that under these conditions also some ill-defined oligomers are formed.

In contrast, reactions carried out in the presence of chloride or acetic acid as additive resulted in much better resolved ^{1}H NMR spectra of the mixture (Figure 5). HRMS-ESI analysis of the resulting solutions showed that the desired $Pt_{12}\mathbf{L}^{\mathbf{SOMe}}{}_{24}$ nanosphere was formed in high selectivity (Figure 6). TBACl addition showed the best resolved ^{1}H NMR spectrum with well-defined signals and excellent selectivity towards the $Pt_{12}\mathbf{L}^{\mathbf{SOMe}}{}_{24}$ assembly based on HRMS-ESI, ^{1}H NMR and DOSY (Figure 6 and S49). Whereas signals that are attributed to the β-pyridine proton and all central benzene protons (Figure 5, right, b–d) are well resolved, the α-pyridine protons (Figure 5, right, a) are split into multiple sets of doublets. Because no other species could be identified using HRMS-ESI, we attribute this splitting to different rotation orientations of the α-pyridines around the platinum centre (Figure S11 and ref. [18]). Interestingly, high purity nanospheres can be formed by either using TBACl or alkyl acids. Analogues experiments using the more flexible $\mathbf{L}^{\mathbf{OMe}}$ in the presence of catalytic amounts of TBACl showed not much difference in the distribution of sphere products that were formed. The ^{1}H NMR spectra were identical as the experiment in absent of additives and HRMS-ESI analysis showed no significant increase in selectivity for the $Pt_{12}\mathbf{L}^{\mathbf{OMe}}{}_{24}$ assembly (Figure 5). The difference in relative energy between the different nanospheres based on $\mathbf{L}^{\mathbf{OMe}}$ is sufficient for palladium-based spheres to generate pure $Pd_{12}L_{24}$ spheres. This similar energy difference observed for the platinum-based analogue does not lead to pure $Pt_{12}\mathbf{L}^{\mathbf{OMe}}{}_{24}$ sphere formation, even if chlorides additives are used. This suggests that labilisation by additives alone is not sufficient for these structures to convert the kinetic traps into the $Pt_{12}\mathbf{L}^{\mathbf{OMe}}{}_{24}$ sphere, but that the thermodynamic destabilisation of the intermediates is required too. This can be achieved by using rigid ligands as demonstrated with $\mathbf{L}^{\mathbf{SOMe}}$.

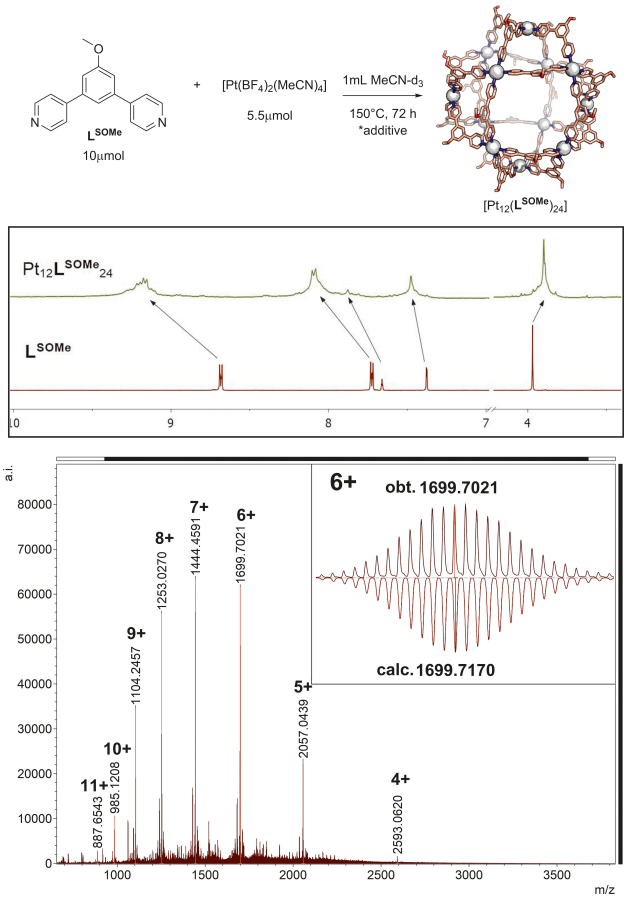

Figure 6. Optimised conditions for the synthesis of exo-functionalised $Pt_{12}L_{24}$ spheres. ^{1}H NMR of the assembly and the applied building block L^{SOMe}. HRMS-ESI of the $Pt_{12}L^{SOMe}{}_{24}$ assembly, top: obtained spectra, bottom: simulated patterns.

To evaluate the functional group-independency of this combined method of chloride-catalysed assembly of $Pt_{12}L_{24}$ cages with rigid ditopic ligands, we applied $\mathbf{L}^{\mathbf{Fu}}$ (nonfunctionalised), $\mathbf{L}^{\mathbf{PEG}}$ (*exo*-functionalised) and $\mathbf{L}^{\mathbf{SOBn}}$ (*endo*-functionalised; Figure 7) as building blocks in sphere formation. Sphere formation using catalytic amounts of TBACl in [D_3]MeCN and high temperatures (150 °C), yield for both rigid building blocks $\mathbf{L}^{\mathbf{Fu}}$ and $\mathbf{L}^{\mathbf{PEG}}$ pure $Pt_{12}L_{24}$ nanospheres as judged by the well-resolved ^{1}H NMR spectrum (Figures S25 and S29). Also, HRMS-ESI confirms the high selectivity for the desired $Pt_{12}\mathbf{L}^{\mathbf{Fu}}{}_{24}$ and $Pt_{12}\mathbf{L}^{\mathbf{PEG}}{}_{24}$ nanospheres as signals corresponding to other spheres were absent (Figures S28 and S30).

In order to introduce *endo* functionalities on spheres which are made up from building blocks without any linkers between the central benzene ring and the pyridine donors, mixing of two building blocks, one without any *endo* functionalisation and one with *endo* functionalisation is required. When the $\mathbf{L}^{\mathbf{SOBn}}$ building block was mixed in a one-to-one ratio with $\mathbf{L}^{\mathbf{SOMe}}$, selective formation of the $Pt_{12}\mathbf{L}^{\mathbf{SOMe}}{}_x\mathbf{L}^{\mathbf{SOBn}}{}_{24-x}$ assemblies was

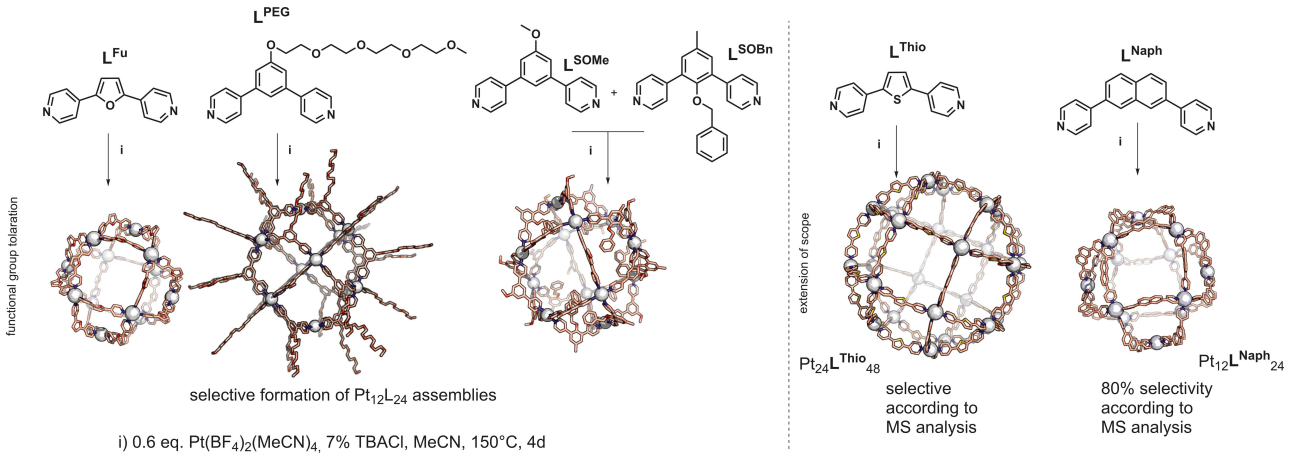

Figure 7. Left: Selective sphere formation with 7 mol% TBACl using differently functionalised building blocks. Right: Formation of self-assemblies using different linker core structures.

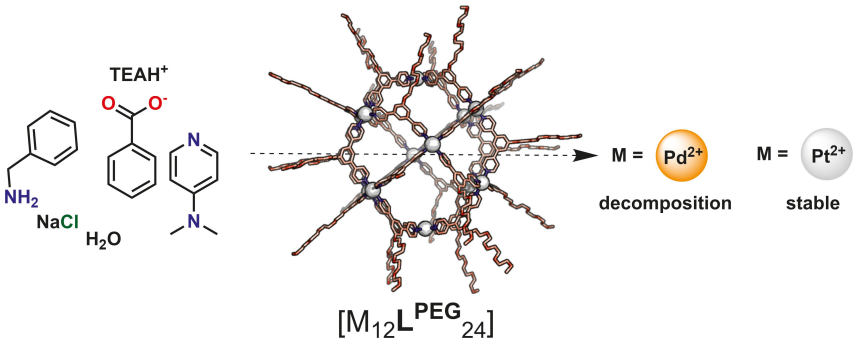

Figure 8. Stability studies performed on $Pt_{12}L^{PEG}{}_{24}$ and $Pd_{12}L^{PEG}{}_{24}$. Stability was measured by using ^{1}H NMR spectroscopy after 24 h.

achieved based on ^{1}H NMR and HRMS-ESI analysis (Figures S31 and S32). The HRMS-ESI show a statistical distribution of the different spheres ($Pt_{12}\mathbf{L}^{SOMe}{}_x\mathbf{L}^{SOBn}{}_{24-x}$) in agreement with a system that shows no self-sorting (Figure S33). Importantly, also for these nanospheres the protocol in the presence of TBACl additive leads to pure $Pt_{12}L_{24}$ nanosphere formation, and none of the smaller spheres were observed in the MS spectra. These experiments provide evidence for the functional-group independency of the design principles. It is important to mention here that the general applicability of this methodology is only ensured if an applied building block posses the following characteristics: 1) it allows solubility of intermediates and the resulting sphere in MeCN, and 2) it destabilises the oligomers and kinetic traps to the same or higher extent as $\mathbf{L}^{SOMe}$. The methodology works worse if one or both of these criteria are not fulfilled. When we attempted sphere formation under identical conditions as described for $\mathbf{L}^{SOMe}$ with $\mathbf{L}^{Naph}$ (Figure 7; which does not dissolve well in MeCN and leads to precipitation of some intermediates), a lower selectivity was achieved for the desired $Pt_{12}\mathbf{L}^{Naph}{}_{24}$ assembly (80% as judged by MS analysis, Figure S37). When $\mathbf{L}^{Thio}$ was used for sphere formation (Figure 7; which energetic profile was not considered herein), selective formation of the desired $Pt_{24}\mathbf{L}^{Thio}{}_{48}$ was achieved as judged by MS analysis (Figures S40 and S41). However, the relatively broad ^{1}H NMR spectrum (which is in accordance with analogous previously reported $Pd_{24}L^{Thio}{}_{48}$ assemblies[11e]) does not allow for judgement of the bulk purity (Figure S38). Even though, the presence of oligomeric material cannot be excluded, the desired $Pt_{24}\mathbf{L}^{Thio}{}_{48}$ assembly was formed selectively as judged by MS analysis. A general applicability for other ligand systems requires in general in-depth analysis of the energetic states and design that allow good solubility. However, with the $\mathbf{L}^{SOMe}$ type presented herein, any functionality can be placed on the in- or outside of $Pt_{12}L_{24}$ assemblies, providing an advantage of this method over previously reported design principles.

With a series of $Pt_{12}L_{24}$ nanospheres in hand made based on a new protocol, their kinetic stability was investigated. Because better solubility of the building block and the resulting spheres was expected for $\mathbf{L}^{PEG}$, we chose the nanosphere based on this building block for the stability experiments. A set of different substrates (Figure 8), which represent the additives used to increase dynamicity, were added to a solution containing either $Pt_{12}\mathbf{L}^{PEG}{}_{24}$ or $Pd_{12}\mathbf{L}^{PEG}{}_{24}$. The solutions were stirred for 24 h at room temperature and the stability was studied using ^{1}H NMR. Signals corresponding to the palladium-based systems disappeared and the signals of the free building block $\mathbf{L}^{PEG}$ appeared

under all applied conditions (Figure S54). As such, the $Pd_{12}L^{PEG}_{24}$ nanosphere is not stable in presence of any coordinating substrates. In contrast, the platinum spheres remained intact in presence of the additives. The peaks corresponding to the $Pt_{12}L^{PEG}_{24}$ nanosphere in the ^{1}H NMR did not change, and signals that are typical for the free building block were not visible (Figure S55). As such platinum-based spheres are kinetically stable in the presence of base (DMAP), acetates (benzoic acetate), amines (benzylamine) and halides (NaCl in D_2O) at room temperature, but the same compounds can facilitate cage formation at 150 °C as they somewhat labilise the inert platinum-pyridyl bond.

Conclusion

In summary, we have demonstrated the successful preparation of robust platinum-based nanospheres by using a new protocol. The challenge in making $M_{12}L_{24}$ platinum spheres is that kinetic trapped intermediates can form, prohibiting the formation of pure structures. Such unwanted structures should be avoided. We therefore introduce here the flexibility angle, next to the previously introduced dihedral angle for palladium spheres, to allow the rational design of ligand building blocks that form $Pt_{12}L_{24}$. For some ligands that differ in flexibility range, possible intermediates were computationally analysed to confirm that the rigidity of the applied building blocks leads to larger energy differences between the thermodynamically most stable $Pt_{12}L_{24}$ structure and the smaller intermediates. Under standard conditions a mixture of spheres was still formed, thus indicating that the strong metal-ligand bond does not allow the repair mechanisms required for the formation of the most stable structure. These bonds can be labilised by the presence of additives such chloride and alkyl acids, converting the kinetically trapped intermediates to the desired $Pt_{12}L_{24}$ structures. This was demonstrated for a series of rigid ligands with a small flexibility range. Whereas these additives lead to sufficient dynamicity at elevated temperature to form the thermodynamically most stable structure, the formed assemblies are kinetically stable in presence of these additives at room temperature. The possibilities of how such coordinating additives can influence the outcome of the formation of self-assemblies kinetically together with thermodynamic tuning by using computational investigation yields an ideal starting point for the investigation of other self-assemblies for which enhancement of their stability is demanded.

Acknowledgements

We acknowledge the University of Amsterdam for their kind financial support to RPA sustainable chemistry.

Conflict of Interest

The authors declare no conflict of interest.

Keywords: coordination chemistry · kinetic traps · platinum · self-assembly · supramolecular chemistry

[1] a) A. Pöthig, A. Casini, *Theranostics* **2019**, *9*, 3150–3169; b) A. Schmidt, V. Molano, M. Hollering, A. Pothig, A. Casini, F. E. Kuhn, *Chem. Eur. J.* **2016**, *22*, 2253–2256; c) B. P. Burke, W. Grantham, M. J. Burke, G. S. Nichol, D. Roberts, I. Renard, R. Hargreaves, C. Cawthorne, S. J. Archibald, P. J. Lusby, *J. Am. Chem. Soc.* **2018**, *140*, 16877–16881.

[2] a) V. Marti-Centelles, A. L. Lawrence, P. J. Lusby, *J. Am. Chem. Soc.* **2018**, *140*, 2862–2868; b) R. L. Spicer, A. D. Stergiou, T. A. Young, F. Duarte, M. D. Symes, P. J. Lusby, *J. Am. Chem. Soc.* **2020**, *142*, 2134–2139; c) S. Gonell, X. Caumes, N. Orth, I. Ivanovic-Burmazovic, J. N. H. Reek, *Chem. Sci.* **2019**, *10*, 1316–1321; d) S. H. A. M. Leenders, M. Dürr, I. Ivanović-Burmazović, J. N. H. Reek, *Adv. Synth. Catal.* **2016**, *358*, 1509–1518; e) Q. Q. Wang, S. Gonell, S. H. Leenders, M. Durr, I. Ivanovic-Burmazovic, J. N. Reek, *Nat. Chem.* **2016**, *8*, 225–230; f) S. H. Leenders, R. Gramage-Doria, B. de Bruin, J. N. Reek, *Chem. Soc. Rev.* **2015**, *44*, 433–448; g) C. Tan, D. Chu, X. Tang, Y. Liu, W. Xuan, Y. Cui, *Chem. Eur. J.* **2019**, *25*, 662–672; h) Y. Fang, J. A. Powell, E. Li, Q. Wang, Z. Perry, A. Kirchon, X. Yang, Z. Xiao, C. Zhu, L. Zhang, F. Huang, H. C. Zhou, *Chem. Soc. Rev.* **2019**, *48*, 4707–4730; i) D. Fiedler, D. H. Leung, R. G. Bergman, K. N. Raymond, *Acc. Chem. Res.* **2005**, *38*, 349–358; j) D. Fiedler, R. G. Bergman, K. N. Raymond, *Angew. Chem. Int. Ed.* **2006**, *45*, 745–748; *Angew. Chem.* **2006**, *118*, 759–762; k) D. H. Leung, D. Fiedler, R. G. Bergman, K. N. Raymond, *Angew. Chem. Int. Ed.* **2004**, *43*, 963–966; *Angew. Chem.* **2004**, *116*, 981–984.

[3] a) D. Zhang, T. K. Ronson, Y.-Q. Zou, J. R. Nitschke, *Nat. Chem. Rev.* **2021**, *5*, 168–182; b) J. H. Zhang, S. M. Xie, M. Zi, L. M. Yuan, *J. Sep. Sci.* **2020**, *43*, 134–149; c) S. Rojas, P. Horcajada, *Chem. Rev.* **2020**, *120*, 8378–8415; d) T. Y. Kim, R. A. S. Vasdev, D. Preston, J. D. Crowley, *Chem. Eur. J.* **2018**, *24*, 14878–14890.

[4] a) K. Acharyya, S. Bhattacharyya, H. Sepehrpour, S. Chakraborty, S. Lu, B. Shi, X. Li, P. S. Mukherjee, P. J. Stang, *J. Am. Chem. Soc.* **2019**, *141*, 14565–14569; b) R. Zaffaroni, E. O. Bobylev, R. Plessius, J. I. van der Vlugt, J. N. H. Reek, *J. Am. Chem. Soc.* **2020**, *142*, 8837–8847; c) T. Keijer, T. Bouwens, J. Hessels, Joost N. H. Reek, *Chem. Sci.* **2021**, *12*, 50–70.

[5] a) R. Chakrabarty, P. S. Mukherjee, P. J. Stang, *Chem. Rev.* **2011**, *111*, 6810–6918; b) M. Han, D. M. Engelhard, G. H. Clever, *Chem. Soc. Rev.* **2014**, *43*, 1848–1860; c) B. Li, T. He, Y. Fan, X. Yuan, H. Qiu, S. Yin, *Chem. Commun.* **2019**, *55*, 8036–8059; d) M. Yoshizawa, J. K. Klosterman, M. Fujita, *Angew. Chem. Int. Ed.* **2009**, *48*, 3418–3438; *Angew. Chem.* **2009**, *121*, 3470–3490.

[6] D. Fujita, A. Takahashi, S. Sato, M. Fujita, *J. Am. Chem. Soc.* **2011**, *133*, 13317–13319.

[7] a) D. Preston, S. M. McNeill, J. E. Lewis, G. I. Giles, J. D. Crowley, *Dalton Trans.* **2016**, *45*, 8050–8060; b) R. A. S. Vasdev, L. F. Gaudin, D. Preston, J. P. Jogy, G. I. Giles, J. D. Crowley, *Front. Chem.* **2018**, *6*, 563.

[8] a) S.-F. Xi, L.-Y. Bao, Z.-L. Xu, Y.-X. Wang, Z.-D. Ding, Z.-G. Gu, *Eur. J. Inorg. Chem.* **2017**, *2017*, 3533–3541; b) C. S. Tsang, L. Chen, L. W. Li, S. M. Yiu, T. C. Lau, H. L. Kwong, *Dalton Trans.* **2015**, *44*, 13087–13092.

[9] a) W. M. Bloch, R. Babarao, M. L. Schneider, *Chem. Sci.* **2020**, *11*, 3664–3671; b) M. L. Schneider, O. M. Linder-Patton, W. M. Bloch, *Chem. Commun.* **2020**, *56*, 12969–12972; c) G. A. Craig, P. Larpent, S. Kusaka, R. Matsuda, S. Kitagawa, S. Furukawa, *Chem. Sci.* **2018**, *9*, 6463–6469; d) L. Chen, T. Yang, H. Cui, T. Cai, L. Zhang, C.-Y. Su, *J. Mater. Chem. A* **2015**, *3*, 20201–20209; e) M. J. Prakash, M. Oh, X. Liu, K. N. Han, G. H. Seong, M. S. Lah, *Chem. Commun.* **2010**, *46*, 2049–2051.

[10] a) F. Kaiser, A. Schmidt, W. Heydenreuter, P. J. Altmann, A. Casini, S. A. Sieber, F. E. Kühn, *Eur. J. Inorg. Chem.* **2016**, *2016*, 5189–5196; b) E. Puig, C. Desmarets, G. Gontard, M. N. Rager, A. L. Cooksy, H. Amouri, *Inorg. Chem.* **2019**, *58*, 3189–3195.

[11] a) D. K. Chand, K. Biradha, M. Kawano, S. Sakamoto, K. Yamaguchi, M. Fujita, *Chem. Asian J.* **2006**, *1*, 82–90; b) D. Fujita, Y. Ueda, S. Sato, H. Yokoyama, N. Mizuno, T. Kumasaka, M. Fujita, *Chem.* **2016**, *1*, 91–101; c) K. Harris, Q. F. Sun, S. Sato, M. Fujita, *J. Am. Chem. Soc.* **2013**, *135*, 12497–12499; d) S. Sato, Y. Ishido, M. Fujita, *J. Am. Chem. Soc.* **2009**, *131*, 6064–6065; e) Q. F. Sun, J. Iwasa, D. Ogawa, Y. Ishido, S. Sato, T. Ozeki, Y. Sei, K. Yamaguchi, M. Fujita, *Science* **2010**, *328*, 1144–1147; f) K. Suzuki, M. Tominaga, M. Kawano, M. Fujita, *Chem. Commun.* **2009**, 1638–1640; g) M. Yoneya, S. Tsuzuki, T. Yamaguchi, S. Sato, M. Fujita, *ACS Nano* **2014**, *8*, 1290–1296.

[12] X. Yan, P. Wei, Y. Liu, M. Wang, C. Chen, J. Zhao, G. Li, M. L. Saha, Z. Zhou, Z. An, X. Li, P. J. Stang, *J. Am. Chem. Soc.* **2019**, *141*, 9673–9679.

[13] A. V. Zhukhovitskiy, M. Zhong, E. G. Keeler, V. K. Michaelis, J. E. Sun, M. J. Hore, D. J. Pochan, R. G. Griffin, A. P. Willard, J. A. Johnson, *Nat. Chem.* **2016**, *8*, 33–41.
[14] a) N. Kamiya, M. Tominaga, S. Sato, M. Fujita, *J. Am. Chem. Soc.* **2007**, *129*, 3816–3817; b) T. Kikuchi, S. Sato, D. Fujita, M. Fujita, *Chem. Sci.* **2014**, *5*, 3257; c) T. Kikuchi, S. Sato, M. Fujita, *J. Am. Chem. Soc.* **2010**, *132*, 15930–15932.
[15] a) E. O. Bobylev, D. A. Poole III, B. de Bruin, J. N. H. Reek, *Chem. Sci.* **2021**, *12*, 7696–7705; b) Z. Li, N. Kishi, K. Hasegawa, M. Akita, M. Yoshizawa, *Chem. Commun.* **2011**, *47*, 8605–8607; c) Y. Sun, C. Chen, J. Liu, P. J. Stang, *Chem. Soc. Rev.* **2020**, *49*, 3889–3919.
[16] a) K. Yamashita, M. Kawano, M. Fujita, *J. Am. Chem. Soc.* **2007**, *129*, 1850–1851; b) K.-i. Yamashita, K.-i. Sato, M. Kawano, M. Fujita, *New J. Chem.* **2009**, *33*, 264.
[17] J. E. M. Lewis, E. L. Gavey, S. A. Cameron, J. D. Crowley, *Chem. Sci.* **2012**, *3*, 778–784.
[18] D. A. Poole, E. O. Bobylev, S. Mathew, J. N. H. Reek, *Chem. Sci.* **2020**, *11*, 12350–12357.

Manuscript received: June 2, 2021
Accepted manuscript online: June 22, 2021
Version of record online: July 14, 2021

